



This paper is published as: Lignos, D.G., Hartloper, A.R., Elkady, A., Deierlein, G.G., Hamburger, R. (2019). "Proposed updates to the ASCE 41 nonlinear modeling parameters for wide-flange steel columns in support of performance-based seismic engineering, Vol. 145(9), pp. 04019083, doi: 10.1061/(ASCE)ST.1943-541X.0002353

26 **Author keywords:** Steel wide-flange columns; ASCE 41; Nonlinear component modeling;  
27 Performance-based seismic engineering; Steel frame buildings; cyclic deterioration; model  
28 uncertainty.

## 29 **Introduction**

30 Performance assessment by nonlinear dynamic (response history) analyses is being  
31 increasingly used for the seismic assessment and design of buildings and other structures. Over  
32 the past decade or so, general guidelines and criteria have been proposed for the use of  
33 nonlinear dynamic analyses of tall buildings (e.g., LATBSDC 2017; PEER 2017) and other  
34 structures (Deierlein et al. 2010). Most recently, the ASCE 7 standard has introduced a new  
35 chapter on nonlinear dynamic analysis for seismic design (ASCE 2017a; Haselton et al. 2017).  
36 While general guidelines for implementation of nonlinear dynamic analyses have advanced,  
37 detailed recommendations and criteria for structural components have not advanced as quickly.  
38 For example, many engineers rely on model parameters in the ASCE 41 standard (ASCE 2014,  
39 2017b), which date back to guidelines developed for nonlinear static (pushover) analyses in the  
40 late 1990s (ATC 1997; FEMA 1997a; b).

41 In the last decade, guidelines geared to nonlinear dynamic analysis of steel and concrete  
42 buildings have been developed, including updated component hysteretic models that explicitly  
43 capture cyclic strength and stiffness deterioration (PEER/ATC 2010). These models reflected  
44 the most recent findings from laboratory testing of steel beams in pre-qualified beam-to-  
45 column connections (FEMA 2000; Lignos and Krawinkler 2011) that were mainly tested as  
46 part of the SAC joint venture program. Due to the fairly limited experimental data available at  
47 the time, it was recognized that updated modeling recommendations should be provided to  
48 properly model the hysteretic response of steel columns subjected to seismic loading  
49 (PEER/ATC 2010; Hamburger et al. 2016).

50 More recently, several full-scale experiments have been conducted to characterize the  
51 hysteretic behavior of steel columns under multi-axis cyclic loading (Newell and Uang 2008;  
52 Suzuki and Lignos 2015, 2017; Lignos et al. 2016; Ozkula et al. 2017; Elkady and Lignos  
53 2018a). Although these tests revealed that the plastic deformation capacity of steel columns is  
54 strongly influenced by the cross-section and member slenderness as well as the applied axial  
55 load on the column, the ASCE 41-13 skeleton curve deformation parameters do not properly

56 capture these dependencies. This has been also recognized by practicing engineers (Bech et al.  
57 2015).

58 The ASCE 41-13 standard treats steel columns as force-controlled elements (i.e., zero  
59 plastic deformation capacity) when they are subjected to compressive axial load demands of  
60 more than 50%  $P_{CL}$  (where  $P_{CL}$  is the lower-bound axial compressive strength of a steel column  
61 as defined in AISC-341-16 (AISC 2016a)). This limit may lead into seismic retrofit solutions  
62 that often times are needlessly costly (Bech et al. 2015). On the other hand, experimental  
63 evidence and corroborating continuum finite element simulations (Newell and Uang 2008;  
64 Elkady and Lignos 2015, 2018a, 2018b; Lignos et al. 2016) suggest that seismically compact  
65 steel columns as per AISC-341-16 (AISC 2016a) can develop appreciable plastic deformation  
66 capacities even at relatively high compressive axial load demands. Although the recently  
67 published ASCE 41-17 provisions (ASCE 2017b) raised the associated limit for force-  
68 controlled column elements to 50% $P_{ye}$  ( $P_{ye}$  is the axial yield strength and is calculated based  
69 on expected steel material properties) or less, depending on the section compactness, there is  
70 no background information to substantiate such change.

71 Steel-framed structures are often subjected to bidirectional loading due to three dimensional  
72 (3D) ground motion shaking. Similarly, end (i.e., corner) columns of steel moment resisting  
73 frames (MRFs) may experience large fluctuations of axial load demands due to dynamic  
74 overturning effects; hence, their hysteretic behavior is different than that of adjacent interior  
75 steel MRF columns within the same MRF story (Suzuki and Lignos 2015). In particular,  
76 interior steel MRF columns do not experience axial load fluctuations due to overturning forces.  
77 The ASCE 41-17 (ASCE 2017b) provisions do not provide explicit guidance on how to address  
78 the aforementioned two effects.

79 Despite the fact that both FEMA 273/274 (FEMA 1997a; b) and ASCE 41-17 (ASCE  
80 2017b) did not intend for the use of first and/or second cycle component curves in nonlinear  
81 dynamic analysis, absent of other established hysteretic models, engineers often apply the  
82 ASCE 41 component models for dynamic analyses (Hamburger et al. 2016). Although this  
83 issue was explicitly addressed for steel beams (PEER/ATC 2010; Lignos and Krawinkler 2011)  
84 with the use of hysteretic models that incorporate cyclic deterioration in strength and stiffness  
85 (e.g., Ibarra et al. 2005), it still remains a challenge for steel columns. This requires sufficient  
86 monotonic data as well as data from different cyclic loading histories that represent the seismic  
87 demands induced in steel frame buildings by different earthquakes and seismic intensities

88 (Krawinkler 2009; Maison and Speicher 2016). It also requires a sense of the associated  
89 uncertainty for the first-cycle and monotonic backbone input model parameters such that load  
90 and resistance factors can be applied to the associated seismic demands (computed from  
91 analysis). Furthermore, acceptance criteria for both deformation- and force-controlled elements  
92 can be defined in a similar manner with Chapter 16 of ASCE 7-17 (ASCE 2017b).

93 This paper addresses the aforementioned deficiencies by utilizing the available experimental  
94 data, complemented with high-fidelity continuum finite element (CFE) simulations on steel  
95 wide-flange columns. In conjunction, detailed background information and refined nonlinear  
96 modeling recommendations are proposed for the ASCE 41 standard. These include updating  
97 the parameters of the ASCE 41 component model, as well as characterizing the monotonic  
98 response of steel columns (i.e., monotonic backbone curves). The above are achieved in the  
99 form of empirical regression models that can be effectively used in engineering practice.  
100 Recommendations are also made for modeling the cyclic deterioration in strength and stiffness  
101 by utilizing a commonly used phenomenological deterioration model. This paper comprises  
102 part of the work carried out under the ATC-114 project funded by the National Institute of  
103 Standards and Technology (NIST) to propose updated recommendations for all four major  
104 structural materials (Hamburger et al. 2017) as well as guidelines for nonlinear structural  
105 analysis and design of buildings with steel moment frames (Deierlein et al. 2017, 2018).

## 106 **Component Model Description**

107 Figure 1a shows the moment-rotation relation of two nominally identical columns (termed as  
108 "Test data") tested under monotonic and symmetric cyclic lateral loading histories (Suzuki and  
109 Lignos 2015). The first cycle-envelope curve is derived as a series of secants connecting the  
110 peaks of each first-cycle loading excursion of a symmetric loading history in the positive and  
111 negative loading direction. The idealized multi-linear monotonic backbone and first-cycle  
112 envelope curves are superimposed in the same figure (plotted in dashed lines). Although the  
113 first-cycle envelope curve is loading-history dependent (FEMA 2009; Krawinkler 2009), it is  
114 typically used in nonlinear static analysis so as the effects of cyclic deterioration in strength  
115 and stiffness are implicitly reflected in the member's response. On the other hand, a member's  
116 monotonic backbone curve is considered as a unique property. It can be used for nonlinear  
117 dynamic analysis procedures provided that the employed component hysteretic model

118 explicitly simulates the effects of cyclic deterioration in strength and stiffness (e.g., Ibarra et  
119 al. 2005; Krishnan 2010; Sivaselvan 2013).

120 Referring to Fig. 1b, the modeling parameters of the first-cycle envelope curve are  
121 distinguished from those of the monotonic backbone with a superscript asterisk (\*). The  
122 effective elastic stiffness,  $K_e$  of a steel column considers both its flexural and shear  
123 deformations. The yield point is defined by the effective yield strength,  $M_y^*$ , and the  
124 corresponding yield rotation,  $\theta_y^*$ . In the post-yield range, the column hardens prior to reaching  
125 its maximum flexural strength,  $M_{max}^{(*)}$  (i.e., peak response). This point is associated with the  
126 onset of geometric instabilities (i.e., local and/or lateral torsional buckling). The effective yield  
127 strength,  $M_y^*$  is calculated based on a straight line from the peak response ( $M_{max}^{(*)}$ ) that intersects  
128 the elastic slope of the column (i.e., effective stiffness,  $K_e$ ). The slope of this line is such that  
129 the positive and negative areas between the first-cycle envelope (or monotonic curve) and the  
130 line itself are equal in an absolute manner (i.e., equal area rule (Chopra and Goel 2001)). The  
131 pre-peak plastic rotation,  $\theta_p^{(*)}$  defines the column's plastic deformation up to the peak response.  
132 Following the onset of geometric instabilities, the column's response is represented by the post-  
133 peak plastic rotation,  $\theta_{pc}^{(*)}$ . Stabilization of the local buckling amplitude occurs at a residual  
134 moment,  $M_r^{(*)}$  (Krawinkler et al. 1983). Finally, a steel column loses its axial load carrying  
135 capacity at an ultimate rotation,  $\theta_{ult}^{(*)}$ , which is dominated by severe axial shortening (Suzuki  
136 and Lignos 2015).

137 The modified Ibarra-Medina-Krawinkler (IMK) phenomenological component model  
138 (Ibarra et al. 2005; Lignos and Krawinkler 2011) explicitly captures a component's cyclic  
139 deterioration in strength and stiffness. The model assumes that each component has an inherent  
140 reference hysteretic energy property, represented by a parameter  $\Lambda$ . This is known as the  
141 reference cumulative plastic rotation capacity (Lignos and Krawinkler 2011). This property,  
142 which is assumed to be loading-history independent, controls the rate of deterioration in basic  
143 strength,  $\Lambda_s$ , post-peak strength,  $\Lambda_c$ , and unloading stiffness,  $\Lambda_k$  of a structural steel component.

144 Referring to Figs. 1c and 1d, the simulated hysteretic response based on the modified IMK  
145 model is compared with two nominally identical column tests subjected to different loading  
146 histories (Elkady and Lignos 2018a). In brief, the first one is a standard symmetric loading  
147 history (Krawinkler et al. 2000). The second one is asymmetric (termed as collapse protocol)  
148 and imposes a structural component on few inelastic cycles followed by large monotonic

149 pushes (so-called ratcheting) prior to structural collapse. This protocol has been established  
150 based collapse simulation studies of multi-story steel MRFs (Suzuki and Lignos 2014) and has  
151 been successfully used in prior experimental programs to characterize the steel column  
152 hysteretic behavior (Suzuki and Lignos 2015; Lignos et al. 2016; Elkady and Lignos 2018).  
153 The figures suggest that, by utilizing the monotonic backbone curve with properly calibrated  
154 deterioration parameters, the IMK model can simulate the cyclic strength and stiffness  
155 deterioration reasonably well, regardless of the imposed loading history. Therefore, this model  
156 is adopted herein to provide explicit modeling guidelines for steel columns in support of  
157 nonlinear dynamic analysis procedures in a similar manner with steel beams (Lignos and  
158 Krawinkler 2011). The utilized data is also publicly available (<http://resslabtools.epfl.ch/>) for  
159 the development of similar guidelines through the use of other available deterioration models.

#### 160 **Steel Column Database for Component Model Calibration**

161 The component models discussed in the previous section are calibrated with available  
162 experimental data on 151 steel columns (MacRae et al. 1990; Nakashima et al. 1990; Newell  
163 and Uang 2008; Cheng et al. 2013; Chen et al. 2014; Suzuki and Lignos 2015, 2017; Lignos et  
164 al. 2016; Elkady and Lignos 2017, 2018a; Ozkula et al. 2017). The collected tests involve  
165 columns subjected to unidirectional and bidirectional bending under monotonic and reversed  
166 cyclic symmetric lateral loading histories coupled with constant compressive axial load  
167 demands. Datasets including varying axial load demands were also considered (Suzuki and  
168 Lignos 2015, Lignos et al. 2016). Figure 2a shows the ranges of the local flange and web  
169 slenderness ratios,  $b_f/2t_f$  and  $h/t_w$ , respectively, of the collected data. It is common that some  
170 data points overlap one another because multiple tests were conducted on nominally identical  
171 members. The majority of the cross-sections satisfy the compactness limits of highly ductile  
172 members,  $\lambda_{hd}$ , per AISC 341-16 (AISC 2016a). Because the dataset is limited to hot-rolled  
173 cross-sections, there is a relatively strong linear correlation (i.e., correlation coefficient of 0.79)  
174 between  $b_f/2t_f$  and  $h/t_w$ .

175 Figure 2b shows the gravity-induced compressive axial load ratio,  $P_g/P_{ye}$  (where  $P_g$  is the  
176 gravity-induced compressive load) applied on those column tests versus  $h/t_w$ . Notably, several  
177 columns were tested with a  $P_g/P_{ye} > 50\%$  (i.e.,  $P/P_{CL} > 50\%$ ), allowing for a re-assessment of  
178 the ASCE 41-13 (ASCE 2014) compressive axial load limit to the current ASCE 41-17 (ASCE  
179 2017b) limit for force-controlled elements as discussed later on. Referring to Fig. 2, the

180 database is sparsely populated for the purpose of component model calibration. Therefore,  
181 additional data points were generated using high-fidelity CFE simulations to fill the gaps in  
182 both the cross-section slenderness and axial load ranges. This includes nearly 1000 CFE  
183 simulation data points. In brief, the CFE model specifics comprise a number of key  
184 characteristics. In particular, shell elements that are assigned member and local imperfections  
185 within the allowable limits of AISC-360-16 (AISC 2016b) and ASTM (2015), respectively, to  
186 properly trace geometric instabilities associated with local and lateral torsional buckling.  
187 Residual stresses due to hot-rolling are appropriately considered based on the Young (1971)  
188 stress distribution. The steel material inelasticity is simulated through a multiaxial plasticity  
189 model (Voce 1948; Armstrong and Frederick 1966; Chaboche 1989) that captures the  
190 combined effects of the isotropic/kinematic hardening of mild steels. The parameters of this  
191 model are calibrated as discussed in Elkady and Lignos (2018b) and Suzuki and Lignos (2017).  
192 Nonlinear static analysis is used including geometric nonlinearities based on the Newton  
193 solution method. A direct linear equation solver is employed that features a sparse, direct,  
194 Gauss elimination method. The column base degrees of freedom are restrained to mimic ideally  
195 fixed boundary conditions in steel MRFs. On the other hand, the column top end boundary is  
196 flexible mimicking the boundary conditions of first-story steel columns in capacity-designed  
197 steel MRFs. All the CFE simulations were carried out with ABAQUS (ABAQUS 2014). The  
198 validation procedures of the employed FE model including comparisons with a broad range of  
199 test data are discussed in great detail in prior published work by the first and third authors  
200 (Elkady and Lignos 2015, 2018b) as well as an international blind analysis prediction contest  
201 on deep, wide-flange structural steel beam-columns (NIST-ATC 2018).

202 In brief, the considered steel columns utilize cross-section sizes ranging from W12 to W36,  
203 which represent typical member sizes for first story columns in steel frame buildings designed  
204 in high seismic regions of North America. The CFE models are subjected to both symmetric  
205 cyclic and monotonic loading coupled with constant compressive axial load demands ranging  
206 from,  $P_g/P_{ye}$  of 0 to 0.75.

## 207 **Observed Trends of the Component Model Parameters**

208 Prior work (Elkady and Lignos 2015, 2018b, c) underscores the influence of the web  
209 slenderness,  $h/t_w$ , the gravity-induced compressive axial load ratio,  $P_g/P_{ye}$  and the member  
210 slenderness,  $L_b/r_y$  ( $L_b$  is the column's unbraced length;  $r_y$  is the radius of gyration in the

211 column cross-section's weak axis) on the hysteretic response of wide-flange steel columns.  
212 Figure 3 depicts the influence of the above parameters on the deduced parameters of the first-  
213 cycle envelope curve of steel columns. The above geometric and loading parameters are  
214 selected because they were found to be statistically significant to the first cycle envelope and  
215 monotonic backbone input model parameters of a column (Elkady and Lignos 2018b, c). The  
216 data plots distinguish between available physical tests (termed as "Test Data") and the CFE  
217 simulation data (termed as "CFE Data"). The dashed straight lines shown in these figures only  
218 indicate the data trends between the column geometric ( $h/t_w$ ,  $L_b/r_y$ ) and axial loading  
219 parameters ( $P_g/P_{ye}$ ) and the deduced parameters of a column's first-cycle envelope curve. The  
220 established linear trend lines are only used to facilitate the discussion herein. Referring to Fig.  
221 3a, the pre-peak plastic rotation,  $\theta_p^*$ , decreases with increasing  $h/t_w$  due to the earlier onset of  
222 local buckling-induced softening observed in more slender cross-sections. This is exacerbated  
223 with increasing  $P_g/P_{ye}$  (see Fig. 3b). With increasing  $L_b/r_y$ , the cyclic strength deterioration  
224 is accelerated due to coupling of local and lateral torsional buckling (see Fig. 3c). Referring to  
225 Fig. 3b, the decreasing variance in  $\theta_p^*$  with increasing  $P_g/P_{ye}$  highlights the strong influence of  
226 this parameter on  $\theta_p^*$ , an effect that is not reflected in the ASCE 41-13 (ASCE 2014) guidelines.

227 Similar trends are found with respect to the post-peak plastic rotation,  $\theta_{pc}^*$ , although a larger  
228 scatter in the data is observed in this case. This is attributed to the higher dependency of  $\theta_{pc}^*$   
229 on the  $L_b/r_y$  due to coupling of local and lateral torsional buckling in the post-peak response  
230 (Ozkula et al. 2017; Elkady and Lignos 2018a). Notably, the interdependency of  $L_b/r_y$  and  
231  $h/t_w$  on the "a" and "b" ASCE 41-13 component model definitions is neglected. These two  
232 parameters are defined in Fig. 1b.

233 Referring to Fig. 1b, a common value that has been historically employed for the hardening  
234 slope in the post-yield range is 3% of the elastic stiffness or the respective structural component  
235 (ASCE 2014). Steel components subjected to cyclic loading harden due to combined isotropic  
236 and kinematic hardening. This combined hardening effect is dependent on the steel material  
237 type (Kanno 2016). For the employed model discussed herein (see Fig. 1) this effect can only  
238 be inherently represented by a hardening ratio,  $a^* = M_{max}^*/M_y^*$ . Figure 3d shows the relation  
239 of  $a^*$  with respect to  $h/t_w$ . From this figure, stocky columns (i.e.,  $h/t_w \approx 20$ ) can develop a  
240 maximum flexural strength,  $M_{max}^*$  approximately 1.6 times their effective yield strength,  $M_y^*$ ,  
241 due to the delay of local buckling even at large lateral drift amplitudes. This is consistent with

242 observations from full-scale experiments (Newell and Uang 2008). On the other hand, steel  
243 columns with seismically compact but slender cross-sections near the current compactness  
244 limits of highly ductile members (AISC 2016a) exhibit negligible hardening due to the early  
245 onset of geometric instabilities. This becomes more evident in cases that the compressive axial  
246 load demands are larger than  $0.30P_{ye}$ . Referring to the input parameters of the monotonic  
247 backbone curve shown in Fig. 1b, similar trends hold true. In particular, there is a strong  
248 negative relation between  $\theta_p$  and both  $h/t_w$  and  $P_g/P_{ye}$ , as expected. The dependence of  $\theta_p$  on  
249  $L_b/r_y$  is much less pronounced than that observed in the of  $\theta_p^*$ -  $L_b/r_y$  relation. This is due to  
250 the fact that member instabilities of wide-flange steel columns utilizing seismically compact  
251 cross-sections do not typically occur until after the onset of local buckling, which is strongly  
252 associated with a loss of lateral torsional rigidity of a wide-flange member (Elkady and Lignos  
253 2018a). For further details, the reader is referred to Hartloper (2016).

#### 254 **Description of Multiple Regression Model**

255 The most relevant parameters in predicting a wide-flange steel column's first-cycle and  
256 backbone curves are the web slenderness ratio,  $h/t_w$  as defined in AISC-341-16 (AISC 2016a);  
257 the member slenderness ratio,  $L_b/r_y$ ; and the gravity-induced compressive axial load ratio,  
258  $P_g/P_{ye}$ . Accordingly, the proposed empirical multiple regression model is as follows,

$$259 \quad y = \beta_o \left(\frac{h}{t_w}\right)^{\beta_1} \cdot \left(\frac{L_b}{r_y}\right)^{\beta_2} \cdot \left(1 - \frac{P_g}{P_{ye}}\right)^{\beta_3} + \varepsilon \quad (1)$$

260 in which,  $y$  is the predicted response parameter of interest;  $\beta_j$  are the regression coefficients;  
261 and  $\varepsilon$  is the error between the test and predicted responses. The goodness-of-fit for each  
262 regression equation can be partially evaluated based on the coefficient of determination,  $R^2$ ,  
263 and coefficient of variation (COV). The  $R^2$  and COV values are representative of the magnitude  
264 and level of scatter in  $\varepsilon$ , respectively. Although outside the scope of this paper, the reported  
265 COV values can facilitate the quantification of modeling uncertainties on the overall steel  
266 frame building seismic performance in a similar manner discussed in Liel et al. (2009) and  
267 Gokkaya et al. (2016).

268 Although the flange local slenderness,  $b_f/2t_f$  can somewhat affect the response parameters,  
269 it was found to be collinear with  $h/t_w$  for the range of hot-rolled cross-sections included in the  
270 steel column database (see Fig 3a). This argument may not hold true for built up cross-sections,

271 where the strong correlation between  $b_f/2t_f$  and  $h/t_w$  is not necessarily maintained. However,  
272 the focus on the present work is on beam-columns utilizing hot-rolled cross-sections.

273 Stepwise multiple regression analysis (Chatterjee and Hadi 2015) is used to determine the  
274 regression equations' coefficients. The statistical analysis of the regression models is presented  
275 in detail in the following section.

## 276 **Statistical Analysis of the Regression Models**

277 The quality of each regression model is evaluated based on the conditions of the Gauss-Markov  
278 theory (Chatterjee and Hadi 2015). In particular, three conditions are checked for each model:  
279 (1) the mean of the residuals is equal to zero; (2) the residuals have constant variance (i.e.,  
280 homoscedasticity); and (3) no correlation is present among the residuals. Residuals were  
281 calculated for the plastic deformation parameters  $\theta_p$  ( $\theta_p^*$ ),  $\theta_{pc}$  ( $\theta_{pc}^*$ ) the hardening ratios  $\alpha$  ( $\alpha^*$ )  
282 and the residual flexural strength,  $M_r$  ( $M_r^*$ ). The raw residual is utilized for this purpose, which  
283 is defined as the difference between the observed values minus the predicted ones from the  
284 developed regression equations. All statistical tests are conducted considering a significance  
285 level of 5% (i.e.,  $\alpha = 0.05$ ). For brevity, only the statistical analysis of  $\theta_p^*$  is presented herein.  
286 The reader is referred to Hartloper (2016) for further details regarding the rest of the input  
287 model parameters.

288 A Lilliefors test (Lilliefors 1967) is conducted on the residuals of the  $\theta_p^*$  model. The resulting  
289  $p$ -value of about 0.5 confirms the null hypothesis of normally-distributed residuals. This is  
290 supported by visual inspection of the quantile-quantile (i.e., QQ) plot (Chatterjee and Hadi  
291 2015) shown in Fig. 4a. The markers falling close to the dashed line indicate that the residuals  
292 closely follow the normal distribution, as originally assumed in the null hypothesis.

293 The condition of mean of the residuals is assumed to be zero is evaluated through a  $t$ -test.  
294 Based on the residuals of the  $\theta_p^*$  model, the test returned a  $p$ -value  $\approx 1.00$ , indicating that the  
295 residuals have a zero mean. The homoscedasticity of the residuals is visually checked based on  
296 the plot of residuals versus the predicted values. Referring to Fig. 4b, in general, the residuals  
297 have a constant variance over the range of predicted values.

298 Finally, the correlation between residuals and predictors is evaluated based on inspection of  
299 the partial residual plots (Fox 1991). The partial residual plot with respect to  $P_g/P_{ye}$  is shown  
300 in Fig. 4c. A relationship is evident between these two parameters, as indicated by the dashed

301 trend line. The regression equation generally underestimates the  $\theta_p^*$  for high compressive axial  
302 load ratios (i.e.,  $P_g/P_{ye} > 35\%$ ), and overestimates in between. To preserve the form of the  
303 proposed equations for simplicity, and to ensure rational predictions for the pre-peak plastic  
304 rotation at moderate axial load levels, a limit of  $\theta_p^* \leq 0.1$  rad is imposed to the respective  
305 equation. Similar restrictions are placed on the rest of the empirical equations where this issue  
306 is encountered.

## 307 **Proposed Equations for Predicting Component Model Parameters for Wide Flange Steel** 308 **Columns**

309 This section provides equations to estimate each of the proposed component models'  
310 parameters (see Fig. 1). The dataset used to develop Eqs. (2) through  
311 **Error! Reference source not found.** comprised of structural steel cross sections made of  
312 ASTM A992 Gr. 50 steel (ASTM 2015) or equivalent steel material (i.e.,  $F_{yn} = 345$  MPa). The  
313 ranges of predictor variables in Eqs. (2) through **Error! Reference source not found.** are as  
314 follows:  $3.71 \leq h/t_w \leq 57.5$ ,  $38.4 \leq L_b/r_y \leq 120$ , and  $0.0 \leq P_g/P_{ye} \leq 0.75$ .

### 315 *Flexural strength parameters*

316 The effective yield strength,  $M_y^*$ , is calculated based on the AISC-360-16 (AISC 2016b) P-M  
317 interaction equation adjusted for the effects of cyclic hardening as follows,

$$318 \quad M_y^* = \begin{cases} 1.15 \cdot Z \cdot R_y \cdot F_{yn} \cdot \left(1 - \frac{P_g}{2P_{ye}}\right) & \text{if } P_g/P_{ye} < 0.20 \\ 1.15 \cdot Z \cdot R_y \cdot F_{yn} \cdot \frac{9}{8} \left(1 - \frac{P_g}{P_{ye}}\right) & \text{if } P_g/P_{ye} \geq 0.20 \end{cases}, (\text{COV}=0.10) \quad (2)$$

319 in which,  $Z$  is the plastic section modulus of the wide-flange cross-section;  $R_y$  is the expected-  
320 to-nominal yield stress ratio from Table A3.1 per AISC-341-16 (AISC 2016a); and  $F_{yn}$  is the  
321 nominal yield stress of the steel material. Note that  $M_y^*$  is the same for both the proposed  
322 monotonic and first-cycle envelope curves.

323 The peak flexural strength  $M_{max}^{(*)}$  can then be computed as  $M_{max}^{(*)} = a^{(*)} \cdot M_y^*$ , where the  
324 hardening ratio parameters,  $a$  (for the monotonic backbone) and  $a^*$  (for the first-cycle  
325 envelope) are estimated using Eqs. (3) or (4), respectively. An upper bound of 1.3 is enforced  
326 to limit the amount of cyclic hardening in columns with stocky cross-sections undergoing low  
327 compressive axial load demands. This limit is rational for A992 Gr. 50 steel or equivalent steels  
328 (Kanno 2016; Sousa and Lignos 2017). The corresponding hardening ratios are as follows,

$$329 \quad a = 12.5 \cdot \left(\frac{h}{t_w}\right)^{-0.2} \cdot \left(\frac{L_b}{r_y}\right)^{-0.4} \cdot \left(1 - \frac{P_g}{P_{ye}}\right)^{0.4} \quad 1.0 \leq a \leq 1.3 \quad (3)$$

$$330 \quad (R^2 = 0.76, COV = 0.1)$$

331

$$332 \quad a^* = 9.5 \cdot \left(\frac{h}{t_w}\right)^{-0.4} \cdot \left(\frac{L_b}{r_y}\right)^{-0.16} \cdot \left(1 - \frac{P_g}{P_{ye}}\right)^{0.2} \quad 1.0 \leq a \leq 1.3 \quad (4)$$

$$333 \quad (R^2 = 0.87, COV = 0.07)$$

334

335 Expressed as a percentage of the effective yield strength, the column's residual flexural  
336 strength,  $M_r$  or  $M_r^*$ , can be estimated by Eqs. (5) and **Error! Reference source not found.**,  
337 respectively,

$$338 \quad M_r = \left(0.5 - 0.4 \cdot \frac{P_g}{P_{ye}}\right) \cdot M_y^* \quad (COV = 0.27) \quad (5)$$

$$339 \quad M_r^* = \left(0.4 - 0.4 \cdot \frac{P_g}{P_{ye}}\right) \cdot M_y^* \quad (COV = 0.35) \quad (6)$$

#### 340 ***Yield deformation***

341 The effective yield rotation,  $\theta_y^*$ , shall be deduced directly from the column's effective yield  
342 strength,  $M_y^*$ , and the elastic stiffness,  $K_e$ . Experiments (Lignos et al. 2016; Ozkula et al. 2017;  
343 Elkady and Lignos 2018a) suggest that the contribution of the shear deformations can reach up  
344 to 30% of the overall column's elastic deformation for standard building configurations.  
345 Therefore, the column's elastic stiffness  $K_e$  can be computed in the same manner with the  
346 flexural stiffness of eccentrically braced frame link beams (Bech et al. 2015). In particular,  
347  $K_e = L^2 K_s K_b / [2(K_s + K_b)]$  in which, the shear and flexural stiffness are  $K_s = GA_w / L$  and  
348  $K_b = 12EI / L^3$ , respectively. If the column is not in double curvature, then  $K_b$  shall be adjusted  
349 accordingly;  $E$  and  $G$  are Young's and the shear modulus, respectively, of the steel material;  
350  $A_w$  is the web area of the wide-flange cross-section as defined in AISC-341-16 (AISC 2016a);  
351  $L$  is the column's length;  $I$  is the moment of inertia of the cross-section with respect to its strong  
352 axis.

#### 353 ***Plastic deformation parameters***

354 The steel column's pre-peak plastic rotation ( $\theta_p$  or  $\theta_p^*$ ) can be estimated as follows,

$$355 \quad \theta_p = 294 \cdot \left(\frac{h}{t_w}\right)^{-1.7} \cdot \left(\frac{L_b}{r_y}\right)^{-0.7} \cdot \left(1 - \frac{P_g}{P_{ye}}\right)^{1.6} \quad \theta_p \leq 0.20 \text{ rad} \quad (7)$$

$$356 \quad (R^2 = 0.89, COV = 0.39)$$

357

$$\theta_p^* = 15 \cdot \left(\frac{h}{t_w}\right)^{-1.6} \cdot \left(\frac{L_b}{r_y}\right)^{-0.3} \cdot \left(1 - \frac{P_g}{P_{ye}}\right)^{2.3} \quad \theta_p^* \leq 0.10rad \quad (8)$$

$$(R^2 = 0.89, COV = 0.31)$$

360

361 Similarly, the post-peak plastic deformation capacity ( $\theta_{pc}$  or  $\theta_{pc}^*$ ), representative of the  
362 column's post-buckling behavior can be estimated as,

$$\theta_{pc} = 90 \cdot \left(\frac{h}{t_w}\right)^{-0.8} \cdot \left(\frac{L_b}{r_y}\right)^{-0.8} \cdot \left(1 - \frac{P_g}{P_{ye}}\right)^{2.5} \quad \theta_p \leq 0.30rad \quad (9)$$

$$(R^2 = 0.91, COV = 0.26)$$

365

$$\theta_{pc}^* = 14 \cdot \left(\frac{h}{t_w}\right)^{-0.8} \cdot \left(\frac{L_b}{r_y}\right)^{-0.5} \cdot \left(1 - \frac{P_g}{P_{ye}}\right)^{3.2} \quad \theta_p \leq 0.10rad \quad (10)$$

$$(R^2 = 0.78, COV = 0.42)$$

368

369 The ultimate rotation ( $\theta_{ult}$  or  $\theta_{ult}^*$ ), representative of the total chord-rotation at which a steel  
370 column loses its axial load carrying capacity, can be estimated as follows,

$$\theta_{ult} = 0.15 \quad (COV = 0.46) \quad (11)$$

$$\theta_{ult}^* = 0.08 \cdot \left(1 - 0.6 \cdot \frac{P_g}{P_{ye}}\right) \quad (COV = 0.51) \quad (12)$$

373 Table 1 summarizes the proposed component model parameters for typical column cross-  
374 sections based on the procedures outlined in this paper. Based on these values, the ratio of the  
375 mean total plastic rotation between the monotonic backbone curve and the first-cycle envelope  
376 curve ( $\theta_{ult} / \theta_{ult}^*$ ) is about 2.6, which is consistent with prior experimental studies conducted  
377 on nominally identical column specimens (Suzuki and Lignos 2015, 2017; Lignos et al. 2016).

### 378 **Reference cumulative plastic rotation capacity**

379 An empirical relation is proposed to compute the reference energy dissipation capacity,  $\Lambda$  of  
380 the modified IMK deterioration model (Ibarra et al. 2005; Lignos and Krawinkler 2011) for  
381 simulating explicitly the cyclic deterioration in strength and stiffness of steel columns in frame  
382 buildings with a concentrated plastic hinge model. For a particular test result, this parameter is  
383 calibrated by minimizing an objective function that consists of the integral of the square  
384 difference between the predicted and the measured moment over the accumulated plastic  
385 rotation. Referring to Figs. 2c and 2d, the simulated column response is based on these

386 calibrations. The proposed equation for computing the  $\Lambda_s$  parameter, which controls the cyclic  
387 basic strength deterioration of a steel column is as follows,

388

$$389 \quad \Lambda_s = \begin{cases} 25,500 \cdot \left(\frac{h}{t_w}\right)^{-2.14} \cdot \left(\frac{L_b}{r_y}\right)^{-0.53} \cdot \left(1 - \frac{P_g}{P_{ye}}\right)^{4.92} \leq 3.0 \text{ if } P_g/P_{ye} \leq 0.35 \\ (R^2 = 0.88, COV = 0.51) \\ 268,000 \cdot \left(\frac{h}{t_w}\right)^{-2.30} \cdot \left(\frac{L_b}{r_y}\right)^{-1.30} \cdot \left(1 - \frac{P_g}{P_{ye}}\right)^{1.19} \leq 3.0 \text{ if } P_g/P_{ye} > 0.35 \\ (R^2 = 0.82, COV = 0.60) \end{cases} \quad (13)$$

390

391 The use of a single equation in this case is not possible because the influence of  $P_g/P_{ye}$  on the  
392 rate of cyclic strength deterioration is not well captured. If a single equation were to be used,  
393 then the  $\Lambda$  values would be under predicted at  $P_g/P_{ye}$  ratios of 5% to 30%, which are commonly  
394 seen in steel MRFs (Suzuki and Lignos 2014). This is not a controlling issue for stocky  
395 columns, where cyclic strength and stiffness deterioration is only a minor issue (Newell and  
396 Uang 2008). Equation (13) suggests that the influence of  $P_g/P_{ye}$  on  $\Lambda_s$  is stronger when  
397  $P_g/P_{ye} \leq 35\%$  than  $P_g/P_{ye} > 35\%$ . The reason is that in the former, for small axial load ratios,  
398 web local buckling is partially restrained because the neutral axis is typically in the web of the  
399 respective cross-section; while in the latter, the neutral axis is typically in the cross-section's  
400 flange; thus, the plate buckling resistance is only modestly influenced by  $P_g/P_{ye}$ .

401 Prior calibration studies for steel beams showed that distinguishing the response with  
402 multiple  $\Lambda$  parameters (e.g., for different deterioration modes) does not necessarily increase  
403 the model accuracy (Lignos and Krawinkler 2011). In the case of wide-flange steel columns,  
404 it was found that the post-peak strength and unloading stiffness deterioration parameters  $\Lambda_c$   
405 and  $\Lambda_k$ , respectively, can be estimated as 0.9 times the value of  $\Lambda_s$ .

## 406 Comparison of Proposed Models with Test Data and ASCE 41-13 Modeling Guidelines

407 The sufficiency of the proposed modeling recommendations in predicting the first cycle and  
408 monotonic backbone curves for steel wide-flange columns is demonstrated through meaningful  
409 comparisons with representative test data. The parameters  $\theta_p^*$ ,  $\theta_{pc}^*$ , that define the plastic  
410 deformation capacity of a steel column's first-cycle envelope curve are plotted against their  
411 corresponding test/simulation values used in the multiple regression models in Figs. 5a and 5b,

412 respectively. Each of the model parameters show a relatively good fit reflected by the data  
413 points clustered close to the dashed line. This is also supported by the corresponding  $R^2$  values.  
414 Referring to Figs. 5a and b, the increase in the scatter with larger response parameter values is  
415 due to the constant variance in the residuals in the log-log domain (i.e., the ratio of the error-  
416 to-predicted magnitude ratio is constant). Consequently, the error increases as the absolute  
417 value of the response parameter increases. Same observations hold true for the rest of the input  
418 model parameters with reference to Figs. 1 and 2. For this reason, upper bound limits are  
419 imposed in the predicted parameters. Same observations hold true for the  $\Lambda$  values of most  
420 column cross-sections as shown in Fig. 5d.

421 Figure 6 shows the response of a number of tested steel columns subjected to monotonic  
422 and symmetric cyclic loading. In an attempt to provide confidence on the proposed modeling  
423 recommendations, superimposed in the same figure, are the component models based on the  
424 procedures proposed in this paper, as well as those from ASCE 41-13 (ASCE 2014) provisions.  
425 The following observations may be made:

- 426 • The ASCE 41-13 model ignores the shear deformation contributions in the column's  
427 effective stiffness,  $K_e$  calculations; thus  $K_e$  is underpredicted by about 30%, on average.  
428 In that sense, the current ASCE 41-17 refined recommendations are substantiated.
- 429 • Referring to Fig. 6a the proposed steel column monotonic backbone represents fairly  
430 well the experimental data including the post-peak plastic deformation range. The  
431 observed differences in the predicted versus the measured effective yield strength are  
432 due to the material variability associated with the expected-to-measured yield stress.
- 433 • Referring to Figs. 6b and 6d, the proposed first-cycle envelope curve represents  
434 relatively well the measured response of steel columns regardless of the  $h/t_w$  and the  
435 applied  $P_g/P_{ye}$ . On the other hand, the ASCE 41 component model overestimates the  
436 pre-peak plastic deformation of steel columns subjected to  $P_g/P_{ye} = 0.20$  (see Fig. 6b).  
437 This is attributed to the fact that the ASCE 41 component model does not capture the  
438 cross-section local slenderness effects on the pre-peak plastic deformation parameter  
439 "a" as defined in the ASCE 41 modeling recommendations. In addition, the ASCE 41  
440 component model does not directly capture the effect of  $L_b/r_y$  on parameter "a".
- 441 • Referring to Figs. 6c and 6d, steel columns that utilize cross sections within the limits  
442 of highly ductile members as per AISC-341-16 (AISC 2016a) and subjected to  $P_g/P_{ye}$   
443 = 0.50 (i.e.,  $P_g/P_{CL} > 0.50$ ) have an appreciable plastic deformation capacity that is

444 significantly underestimated by the ASCE 41-13 component model that treats such  
445 members as force-controlled elements (i.e., no plastic deformation capacity). This issue  
446 is elaborated in a subsequent section.

- 447 • In contrast to the ASCE 41 model, the gradual reduction in the column's flexural  
448 strength in the post-peak response is captured relatively well by the proposed model.

#### 449 **Modeling Recommendations for Columns Subjected to Bidirectional Lateral Loading**

450 Columns in steel frame buildings undergo biaxial bending demands during 3-dimensional  
451 ground shaking. Figure 7 shows a comparison of the normalized first-cycle envelope curves  
452 for two nominally identical W24x84 columns, subjected to unidirectional and bidirectional  
453 loading histories (Elkady and Lignos 2018a) coupled with a constant compressive axial load.  
454 Notably, the plastic deformation capacity of both specimens is virtually the same. Hence, Eqs.  
455 (7) to (13) should be used without any adjustment due to the biaxial bending effects. On the  
456 other hand, the effective flexural strength parameters of the first-cycle and monotonic  
457 backbone curves should be adjusted by modifying Eq. (2) to account for the axial load-biaxial  
458 bending ( $P$ - $M_x$ - $M_y$ ) interaction. The AISC 360-16 (AISC 2016b) interaction equations shall be  
459 employed for this purpose. It should be stated that this observation may not necessarily hold  
460 true for end steel MRF columns experiencing axial load fluctuations synchronized with  
461 bidirectional lateral loading histories. This issue shall be carefully examined in future related  
462 studies.

#### 463 **Modeling Recommendations for End Columns**

464 End columns in steel MRFs may experience large variations in their axial load demands due to  
465 dynamic overturning effects (Suzuki and Lignos 2014). These variations, about the gravity-  
466 induced compressive load  $P_g$ , can reach about  $\pm 35\%$  of  $P_{ye}$  (Suzuki and Lignos 2014). Figure  
467 8 depicts the average first-cycle envelope of both stocky and slender column cross-sections  
468 subjected to gravity-induced axial load  $P_g$ , plus a transient component  $P$  due to dynamic  
469 overturning effects. For instance, Fig. 8a shows a 4000mm long W24x233 column subjected  
470 to a gravity-induced axial load ratio of  $P_g/P_{ye} = 0.15$  and a transient axial load ratio varying  
471 with respect to the gravity-induced offset from  $P/P_{ye} = -0.15$  in tension to  $P/P_{ye} = 0.75$  in  
472 compression while the lateral drift increases up to 0.07rads. Although the peak compressive

473 axial load demand is  $75\%P_{ye}$  (well above  $50\%P_{CL}$ ) in both columns shown in Fig. 8, stocky  
474 cross-sections ( $h/t_w < 10$ ) are able to sustain considerable inelastic deformation demands  
475 without noticeable strength deterioration (see Fig. 8a) due to local and/or member instabilities  
476 (Newell and Uang 2008). Figure 8b, shows the first-cycle moment-rotation envelope of a  
477 W16x89 column, which comprises a slender but seismically compact cross-section according  
478 to the AISC-341-16 (AISC 2016a) seismic provisions. This member experiences local  
479 buckling-induced softening at much smaller inelastic deformations than the W24x233 column.  
480 However, the associated inelastic deformation capacity of the W16x89 is still appreciable  
481 despite the excessive compressive axial load ratio of  $P/P_{ye}=0.75$  due to the combined gravity  
482 and transient axial load demands coupled with the imposed lateral drift history.

483 Referring to Figure 8, unlike the ASCE 41 component model, the proposed model seems to  
484 predict reasonably well the column's plastic deformation capacity by just considering the  
485 gravity-induced load component ( $P_g/P_{ye}$ ). Same observations hold true for the rest of the data.  
486 In that respect, columns experiencing varying axial load and lateral drift demands may be  
487 modeled based on the procedures outlined in this paper considering only the gravity-induced  
488 axial load ratio,  $P_g/P_{ye}$  and neglecting the transient effects. Ideally, numerical models that  
489 explicitly capture the axial force-bending interaction within the cross-section should be  
490 employed for this purpose (e.g., Krishnan 2010; Suzuki and Lignos 2017; Do and Filippou  
491 2018; Kolwankar et al. 2018). Global instability modes shall also be considered within a  
492 simulation framework. As such, the approaches summarized in Krishnan (2010) may be  
493 employed for frame analyses not involving CFE models. However, the coupling of local and  
494 lateral torsional buckling still remains a challenge to be addressed for frame analysis elements.

## 495 **Proposed Updates for Force-Controlled Elements**

496 Referring to Fig. 9, steel columns with seismically compact cross-sections (i.e.,  $h/t_w < 43$ ) have  
497 considerable pre- and post- peak plastic deformation capacities regardless of the applied axial  
498 compressive load ratio. This is also evident from Fig. 2b for the entire column data set as well  
499 as prior related studies by the first and third authors (Elkady and Lignos 2018b). Accordingly,  
500 it is recommended that the ASCE 41-13 force-controlled limit of  $50\% P_{CL}$  be relaxed to  $60\%$   
501  $P_{ye}$  for wide-flange steel columns with  $h/t_w \leq 43$  and  $L_b/r_y \leq 120$ . At compressive axial load  
502 demands near  $P/P_{ye} > 60\%$ , steel columns may be very close to their lower-bound

503 compressive strength,  $P_{CL}$ , especially in the presence of geometric imperfections due to  
504 fabrication/erection. This substantiates the refined limit for force-controlled column elements  
505 according to the ASCE 41-17 standard.

## 506 **Conclusions**

507 This paper provides comprehensive recommendations for nonlinear modeling of wide-flange  
508 steel columns for performance-based seismic assessment of new and existing steel frame  
509 buildings. Two sets of empirical parameters for concentrated hinge models are proposed. The  
510 new model parameters are calibrated to testing and high-fidelity continuum finite element  
511 analyses of wide-flange steel columns. The empirical formulations predict the monotonic and  
512 first-cycle envelope curves of wide flange steel columns in their pre- and post-peak nonlinear  
513 response and can be directly used in nonlinear dynamic and static analysis procedures,  
514 respectively. Recommendations on how to explicitly simulate the cyclic deterioration in  
515 strength and stiffness of steel columns are also provided through the calibration of a widely  
516 used phenomenological deterioration model for frame analysis studies. The proposed first-  
517 cycle envelope curves are directly compared with the ASCE 41 component model for steel  
518 columns. The main findings are summarized as follows:

- 519 • The effective yield strength  $M_y^*$  used in both the first-cycle envelope and monotonic  
520 backbone curves is, on average, 1.15 times the expected plastic resistance of steel  
521 columns reduced by the effects of the gravity induced axial load ratio based on the  
522 AISC-360-16 (AISC 2016b) uniaxial or biaxial bending-axial load interaction  
523 equations for unidirectional or bidirectional lateral loading, respectively.
- 524 • The test data suggest that shear deformations may contribute up to 30% to the effective  
525 elastic stiffness,  $K_e$  of a steel column. Therefore, both flexural and shear deformations  
526 shall be considered in the elastic stiffness computations of steel columns.
- 527 • The axial load ratio,  $P_g/P_{ye}$ , is the primary contributor to the pre-peak plastic rotation,  
528  $\theta_p^{(*)}$  post-peak plastic rotation,  $\theta_{pc}^{(*)}$ , the post-yield hardening ratio  $a^{(*)} = M_{max}^{(*)}/M_y^*$   
529 and the deterioration parameter  $\Lambda$  of hot-rolled wide flange steel columns, followed by  
530 the cross-section's web local slenderness,  $h/t_w$ . Of somewhat importance is the  
531 member slenderness ratio,  $L_b/r_y$  especially in the post-peak column response due to  
532 coupling of local and lateral torsional buckling. The ASCE 41-13 component model for

533 steel columns does not directly capture these effects on the pre-peak plastic deformation  
534 parameter " $a$ ".

- 535 • The ratio of the mean total plastic rotation of a column's monotonic backbone curve to  
536 that of its first-cycle envelope curve is about 2.6.
- 537 • The ultimate rotation,  $\theta_{ult}$  at which a steel column loses its axial load carrying capacity  
538 under cyclic loading is strongly influenced by  $P_g/P_{ye}$  and it is on average 2 to 3 times  
539 less than that of the same column subjected to monotonic loading.
- 540 • Although bidirectional lateral loading has an apparent effect on the column's effective  
541 flexural strength  $M_y^*$ , it does not practically influence the column's plastic deformation  
542 capacity. However, this observation shall be examined carefully for end steel MRF  
543 columns experiencing axial load fluctuations due to dynamic overturning effects  
544 synchronized with bidirectional lateral loading histories.
- 545 • It was found that end columns subjected to varying axial load demands can be modeled  
546 reasonably well by only considering  $P_g/P_{ye}$  and neglecting the transient axial load  
547 component due to dynamic overturning effects. However, additional nonlinear building  
548 simulations are required to further validate this statement.
- 549 • Data from experiments and corroborating finite element analyses suggests that steel  
550 columns with cross sections within the limits of highly ductile members as per AISC-  
551 341-16 (AISC 2016a) have an appreciable plastic deformation capacity even in cases  
552 that  $P_g/P_{CL} > 0.50$ . Accordingly, it is recommended that the ASCE 41-13 force-  
553 controlled limit of 50%  $P_{CL}$  be relaxed to 60%  $P_{ye}$  for wide flange steel columns with  
554  $h/t_w \leq 43$  and  $L_b/r_y \leq 120$ . In that respect, the adopted change in the recent ASCE 41-  
555 17 provisions is deemed to be rational.

556 The conclusions of this paper are based on testing data and continuum finite element analyses  
557 of a wide range of hot-rolled column cross-sections made of A992 Gr. 50 steel or equivalent.  
558 The proposed recommendations shall be used with caution when built-up column cross-  
559 sections are employed. Comprehensive system level studies should be conducted to further  
560 quantify the influence of the proposed modeling recommendations on the overall seismic  
561 behavior of steel frame buildings. For selected case study steel frame buildings, such studies  
562 have been conducted and are summarized in Hamburger et al. (2017).

## 563 Acknowledgements

564 The work forming the basis for this publication was conducted pursuant to a contract with the  
565 National Institute of Standards and Technology (Contract No. 1140-22-431). The substance of  
566 such work is dedicated to the public. The authors are solely responsible for the accuracy of  
567 statements or interpretations contained in this publication. No warranty is offered with regard  
568 to the results, findings and recommendations contained herein, either by the National Institute  
569 of Standards and Technology, or the Applied Technology Council, its directors, members or  
570 employees. These organizations and individuals do not assume any legal liability or  
571 responsibility for the accuracy, completeness, or usefulness of any of the information, product  
572 or processes included in this publication. The authors gratefully acknowledge co-authors and  
573 project review panel of the NIST project; Jon Heintz, Ayse Hortacsu, Veronica Cedillos and  
574 ATC colleagues for managing the project and editing the final guidelines; and Steven L.  
575 McCabe and colleagues at NIST for their input and guidance throughout the project  
576 development process. Additional funding for the third author was provided by the Swiss  
577 National Science Foundation (Project No. 200021\_169248). Any opinions expressed in the  
578 paper are those of the authors and do not necessarily reflect the views of sponsors.

## 579 References

- 580 ABAQUS. (2014). "ABAQUS user's manual." Version 6.14, Providence, R.I.
- 581 AISC. (2016a). *Seismic provisions for structural steel buildings, ANSI/AISC 341-16*. American  
582 Institute of Steel Construction, Chicago, Illinois, United States.
- 583 AISC. (2016b). *Specification for structural steel buildings, ANSI/AISC 360-16*. American  
584 Institute of Steel Construction, Chicago, Illinois, United States.
- 585 Armstrong, P.J., Frederick, C.O. (1966). "A mathematical representation of the multiaxial  
586 bauschinger effect." Technical Report No. RD/B/N 731, Berkeley Nuclear Laboratories,  
587 Berkeley, California.
- 588 ASCE. (2014). *Seismic evaluation and retrofit of existing buildings*, American Society of Civil  
589 Engineers, Reston, Virginia.
- 590 ASCE. (2017a). *Minimum design loads for buildings and other structures*, American Society  
591 of Civil Engineers, Reston, Virginia.
- 592 ASCE. (2017b). *Seismic evaluation and retrofit of existing buildings*, American Society of  
593 Civil Engineers, Reston, Virginia.
- 594 ASTM. (2015). "Standard specification for structural steel shapes." ASTM A992/A992M-11.  
595 West Conshohocken, PA: ASTM.
- 596 ATC. (1997). *Guidelines and commentary for seismic rehabilitation of buildings, FEMA*

This paper is published as: Lignos, D.G., Hartloper, A.R., Elkady, A., Deierlein, G.G., Hamburger, R. (2019). "Proposed updates to the ASCE 41 nonlinear modeling parameters for wide-flange steel columns in support of performance-based seismic engineering, Vol. 145(9), pp. 04019083, doi: 10.1061/(ASCE)ST.1943-541X.0002353

- 597 273/274. Federal Emergency Management Agency, Washington, DC.
- 598 Bech, D., Tremayne, B., and Houston, J. (2015). "Proposed changes to steel column evaluation  
599 criteria for existing buildings." *Proceedings ATC/SEI 2nd Conference on Improving the*  
600 *Seismic Performance of Existing Buildings and Other Structures*, San Francisco, California,  
601 United States, 255–272.
- 602 Chaboche, J.L. (1989). "Constitutive equations for cyclic plasticity and cyclic viscoplasticity."  
603 *International Journal of Plasticity*, 5(3), 247-302.
- 604 Chatterjee, S., and Hadi, A. S. (2015). *Regression analysis by example*. John Wiley & Sons.
- 605 Chen, Y. Y., Niu, L., and Cheng, X. (2014). "Hysteretic behaviour of H steel columns with  
606 large width-thickness ratios under bi-axis moments." *Proceedings 10th National*  
607 *Conference on Earthquake Engineering (10NCEE)*, 21–25, Anchorage, Alaska, USA.
- 608 Cheng, X., Chen, Y., and Pan, L. (2013). "Experimental study on steel beam–columns  
609 composed of slender H-sections under cyclic bending." *Journal of Constructional Steel*  
610 *Research*, 88, 279–288.
- 611 Deierlein, G. G., Bono, S., Malley, J., O., Mazzoni, S., and Uang, C.-M. (2017). *Guidelines for*  
612 *nonlinear structural analysis for design of buildings: Part IIa - Steel moment frames*, Report  
613 No. NIST GCR 17-917-46v2, National Institute of Standards and Technology (NIST), U.S.  
614 Department of Commerce, Washington, DC ([https://doi.org/10.6028/NIST.GCR.17-917-](https://doi.org/10.6028/NIST.GCR.17-917-46v2)  
615 [46v2](https://doi.org/10.6028/NIST.GCR.17-917-46v2)).
- 616 Deierlein, G. G., Lignos, D. G., Bono, S., and Kanvinde, A. (2018). "Guidelines on nonlinear  
617 dynamic analysis for steel moment frames." *Proceedings 11th National Conference in*  
618 *Earthquake Engineering*, Earthquake Engineering Research Institute (EERI), Los Angeles.
- 619 Deierlein, G. G., Reinhorn, A. M., and Willford, M. R. (2010). *Nonlinear structural analysis*  
620 *for seismic design*, NEHRP Seismic Design Technical Brief No. 4, NEHRP Seismic Design  
621 Technical Brief No. 4, National Institute of Standards and Technology, Gaithersburg, MD.
- 622 Do, T. N., and Filippou, F. C. (2018). "A damage model for structures with degrading  
623 response." *Earthquake Engineering & Structural Dynamics*, 47(2), 311–332.
- 624 Elkady, A., and Lignos, D. G. (2015). "Analytical investigation of the cyclic behavior and  
625 plastic hinge formation in deep wide-flange steel beam-columns." *Bulletin of Earthquake*  
626 *Engineering*, 13(4), 1097–1118.
- 627 Elkady, A., and Lignos, D. G. (2018a). "Full-scale testing of deep wide-flange steel columns  
628 under multiaxis cyclic loading: Loading sequence, boundary effects, and lateral stability  
629 bracing force demands." *ASCE Journal of Structural Engineering*, 144(2), 04017189.
- 630 Elkady, A., and Lignos, D. G. (2018b). "Improved seismic design and nonlinear modeling  
631 recommendations for wide-flange steel columns." *ASCE Journal of Structural Engineering*,  
632 144(9), 04018162.
- 633 Elkady, A., Ghimire, S., and Lignos, D.G. (2018c). "Fragility curves for wide-flange steel  
634 columns and implications on building-specific earthquake-induced loss assessment."  
635 *Earthquake Spectra* (in-press).
- 636 Elkady, A., and Lignos, D.G. (2017). "Full-scale cyclic testing of deep slender wide-flange  
637 steel beam-columns under unidirectional and bidirectional lateral drift demands."  
638 *Proceedings 16th World Conference on Earthquake Engineering (16WCEE)*, International

- 639 Association of Earthquake Engineering, Santiago, Chile.
- 640 FEMA. (1997a). *NEHRP Guidelines for the seismic rehabilitation of buildings*. Report FEMA-
- 641 273, Federal Emergency Management Agency, Washington, DC.
- 642 FEMA. (1997b). *NEHRP Commentary on the guidelines for the seismic rehabilitation of*
- 643 *buildings*. Report FEMA-274, Federal Emergency Management Agency, Washington, DC
- 644 FEMA. (2000). *State of the art report on connection performance*. Report FEMA-355D,
- 645 Federal Emergency Management Agency, Washington, DC.
- 646 FEMA. (2009). *Effects of strength and stiffness degradation on seismic response*. Report No.
- 647 FEMA P440A, Federal Emergency Management Agency, Washington, DC.
- 648 Fox, J. (1991). *Regression Diagnostics: An Introduction*. SAGE.
- 649 Gokkaya, B. U., Baker, J. W., and Deierlein, G. G. (2016). "Quantifying the impacts of
- 650 modeling uncertainties on the seismic drift demands and collapse risk of buildings with
- 651 implications on seismic design checks." *Earthquake Engineering & Structural Dynamics*,
- 652 45(10), 1661–1683.
- 653 Hamburger, R., Deierlein, G., Lehman, D., Lowes, L., Shing, B., Van de Lindt, J., Lignos, D.,
- 654 and Hortacsu, A. (2016). "ATC-114 next-generation hysteretic relationships for
- 655 performance-based modeling and analysis." *Proceedings of the SEAOC Convention*,
- 656 Structural Engineers Association of California.
- 657 Hamburger, R. O., Deierlein, G. G., Lehman, D. E., Lignos, D., G., Lowes, L. N., Pekelnicky,
- 658 R. G., Shing, P.-S. B., Somers, P., and Van de Lindt, J. W. (2017). *Recommended modeling*
- 659 *parameters and acceptance criteria for nonlinear analysis in support of seismic evaluation,*
- 660 *retrofit, and design*, Report No. NIST GCR 17-917-45, National Institute of Standards and
- 661 Technology (NIST), U.S. Department of Commerce, Washington, DC
- 662 (<https://doi.org/10.6028/NIST.GCR.17-917-45>).
- 663 Hartloper, A. R. (2016). "Updates to the ASCE-41-13 nonlinear modelling provisions for
- 664 performance-based seismic assessment of new and existing steel moment resisting frames."
- 665 Master Thesis, McGill University, Montreal, Quebec, Canada.
- 666 Haselton, C. B., Baker, J. W., Stewart, J. P., Whittaker, A. S., Luco, N., Fry, A., Hamburger,
- 667 R. O., Zimmerman, R. B., Hooper, J. D., Charney, F. A., and Pekelnicky, R. G. (2017).
- 668 "Response history analysis for the design of new buildings in the NEHRP provisions and
- 669 ASCE/SEI 7 standard: Part I - overview and specification of ground motions." *Earthquake*
- 670 *Spectra*, 33(2), 373-395.
- 671 Ibarra, L. F., Medina, R. A., and Krawinkler, H. (2005). "Hysteretic models that incorporate
- 672 strength and stiffness deterioration." *Earthquake Engineering & Structural Dynamics*,
- 673 34(12), 1489–1511.
- 674 Kanno, R. (2016). "Advances in steel materials for innovative and elegant steel Structures in
- 675 Japan—A review." *Structural Engineering International*, 26(3), 242–253.
- 676 Kolwankar, S., Kanvinde, A., Kenawy, M., Lignos, D.G., Kunnath, S. (2018). "Simulating
- 677 local buckling-induced softening in steel members using an equivalent nonlocal material
- 678 model in displacement-based fiber elements." *ASCE Journal of Structural Engineering*,
- 679 144(10), 04018192.
- 680 Krawinkler, H. (2009). "Loading histories for cyclic tests in support of performance assessment

- 681 of structural components." *Proceedings 3rd International Conference on Advances in*  
682 *Experimental Seismic Engineering*, Pacific Earthquake Engineering Research Center  
683 Annual Conference (PEER), San Francisco, California.
- 684 Krawinkler, H., Zohrei, M., Irvani, B. L., Cofie, N., and Tamjed, H. H. (1983).  
685 *Recommendation for experimental studies on the seismic behavior of steel components and*  
686 *materials*. Report No. 61, The John A. Blume Earthquake Engineering Center, Stanford  
687 University, Stanford, California.
- 688 Krishnan, S. (2010). "Modified elastofiber element for steel slender column and brace  
689 modeling." *ASCE Journal of Structural Engineering*, 136(11), 1350–1366.
- 690 LATBSDC. (2017). "An alternative procedure for seismic analysis and design of tall buildings  
691 located in the Los Angeles region, 2017 Edition." Los Angeles Tall Building Structural  
692 Design Council (<http://www.tallbuildings.org/>).
- 693 Liel, A. B., Haselton, C. B., Deierlein, G. G., and Baker, J. W. (2009). "Incorporating modeling  
694 uncertainties in the assessment of seismic collapse risk of buildings." *Structural Safety*,  
695 31(2), 197–211.
- 696 Lignos, D. G., Cravero, J., and Elkady, A. (2016). "Experimental investigation of the hysteretic  
697 behavior of wide-flange steel columns under high axial load and lateral drift demands."  
698 *Proceedings 11th Pacific Structural Steel Conference*, Shanghai, China.
- 699 Lignos, D. G., and Krawinkler, H. (2011). "Deterioration modeling of steel components in  
700 support of collapse prediction of steel moment frames under earthquake loading." *ASCE*  
701 *Journal of Structural Engineering*, 137(11), 1291–1302.
- 702 Lilliefors, H. W. (1967). "On the Kolmogorov-Smirnov test for normality with mean and  
703 variance unknown." *Journal of the American Statistical Association*, 62(318), 399–402.
- 704 MacRae, G. A., Carr, A. J., and Walpole, W. R. (1990). "The seismic response of steel frames."  
705 PhD Thesis, University of Canterbury, Christchurch, New Zealand.
- 706 Maison, B. F., and Speicher, M. S. (2016). "Loading protocols for ASCE 41 backbone curves."  
707 *Earthquake Spectra*, 32(4), 2513–2532.
- 708 Nakashima, M., Takanashi, K., and Kato, H. (1990). "Test of steel beam-columns subject to  
709 sidesway." *ASCE Journal of Structural Engineering*, 116(9), 2516–2531.
- 710 Newell, J., and Uang, C.-M. (2008). "Cyclic behavior of steel wide-flange columns subjected  
711 to large drift." *ASCE Journal of Structural Engineering*, 134(8), 1334–1342.
- 712 NIST-ATC. (2018). "NIST-ATC blind prediction contest on deep, wide-flange structural steel  
713 beam-columns." Web Page: <https://www.atcouncil.org/atc-106-blind-contest>.
- 714 Ozkula, G., Harris, J., and Uang, C.-M. (2017). "Observations from cyclic tests on deep, wide-  
715 flange beam-columns." *Engineering Journal*, 54(1), 45–59.
- 716 PEER. (2017). *Guidelines for performance-based seismic design of tall buildings*, PEER  
717 *Report 2017/06*. Pacific Earthquake Engineering Research Center, University of California,  
718 Berkeley.
- 719 PEER/ATC. (2010). *Guidelines for performance-based seismic design of Tall Buildings*.  
720 Report No. ATC 72-1, Pacific Earthquake Engineering Research Center, University of  
721 California, Berkeley.
- 722 Sivaselvan, M. V. (2013). "Hysteretic models with stiffness and strength degradation in a

This paper is published as: Lignos, D.G., Hartloper, A.R., Elkady, A., Deierlein, G.G., Hamburger, R. (2019). "Proposed updates to the ASCE 41 nonlinear modeling parameters for wide-flange steel columns in support of performance-based seismic engineering, Vol. 145(9), pp. 04019083, doi: 10.1061/(ASCE)ST.1943-541X.0002353

- 723 mathematical programming format." *International Journal of Non-Linear Mechanics*, 51,  
724 10–27.
- 725 Sousa, A. C., and Lignos, D. G. (2017). *On the inverse problem of classic nonlinear plasticity*  
726 *models-An application to cyclically loaded structural steels*. Technical Report No. 231968,  
727 Resilient Steel Structures Laboratory (RESSLab), École Polytechnique Fédérale de  
728 Lausanne, Lausanne.
- 729 Suzuki, Y., and Lignos, D. G. (2014). "Development of loading protocols for experimental  
730 testing of steel columns subjected to combined lateral drift and high axial load."  
731 *Proceedings 10th National Conference on Earthquake Engineering (10th NCEE)*,  
732 Anchorage, Alaska, United States.
- 733 Suzuki, Y., and Lignos, D. G. (2015). "Large scale collapse experiments of wide flange steel  
734 beam-columns." *Proceedings 8th International Conference on Behavior of Steel Structures*  
735 *in Seismic Areas (STESSA)*, Shanghai, China.
- 736 Suzuki, Y., and Lignos, D. G. (2017). "Collapse behavior of steel columns as part of steel frame  
737 buildings: Experiments and numerical models." *Proceedings 16th World Conference of*  
738 *Earthquake Engineering*, Santiago, Chile.
- 739 Voce, E. (1948). "The relationship between the stress and strain for homogeneous  
740 deformation." *Journal of the Institute of Metals*, 74, 537-562.
- 741

**This paper is published as:** Lignos, D.G., Hartloper, A.R., Elkady, A., Deierlein, G.G., Hamburger, R. (2019). "Proposed updates to the ASCE 41 nonlinear modeling parameters for wide-flange steel columns in support of performance-based seismic engineering, Vol. 145(9), pp. 04019083, doi: 10.1061/(ASCE)ST.1943-541X.0002353

**Table 1.** Deterioration modeling parameters for first-cycle curve and monotonic backbone for selected steel wide-flange column cross-sections [values calculated assuming  $L_b = 4500$  mm,  $F_{yn} = 345$  MPa (A992 Gr. 50 steel)]

| Section | $\frac{h}{t_w}$ | $\frac{L_b}{r_y}$ | $P_g/P_{ye} = 0.20$ |            |               |       |              |                 |             | $P_g/P_{ye} = 0.50$ |            |               |       |              |                 |             |
|---------|-----------------|-------------------|---------------------|------------|---------------|-------|--------------|-----------------|-------------|---------------------|------------|---------------|-------|--------------|-----------------|-------------|
|         |                 |                   | $a$                 | $\theta_p$ | $\theta_{pc}$ | $a^*$ | $\theta_p^*$ | $\theta_{pc}^*$ | $\Lambda_s$ | $a$                 | $\theta_p$ | $\theta_{pc}$ | $a^*$ | $\theta_p^*$ | $\theta_{pc}^*$ | $\Lambda_s$ |
| W33x318 | 28.7            | 47.8              | 1.244               | 0.046      | 0.159         | 1.278 | 0.013        | 0.068           | 0.83        | 1.031               | 0.022      | 0.049         | 1.164 | 0.004        | 0.015           | 0.03        |
| W27x235 | 26.2            | 53.2              | 1.214               | 0.049      | 0.157         | 1.300 | 0.015        | 0.069           | 0.96        | 1.006               | 0.023      | 0.049         | 1.186 | 0.005        | 0.015           | 0.04        |
| W24x146 | 33.2            | 58.9              | 1.111               | 0.031      | 0.120         | 1.166 | 0.010        | 0.054           | 0.55        | 1.000               | 0.015      | 0.037         | 1.061 | 0.003        | 0.012           | 0.02        |
| W24x84  | 45.9            | 90.9              | 1.000               | 0.013      | 0.065         | 1.000 | 0.005        | 0.034           | 0.22        | 1.000               | 0.006      | 0.020         | 1.000 | 0.002        | 0.007           | 0.01        |
| W14x370 | 6.9             | 41.5              | 1.300               | 0.200      | 0.300         | 1.300 | 0.100        | 0.100           | 3.00        | 1.300               | 0.200      | 0.172         | 1.300 | 0.045        | 0.050           | 1.09        |
| W14x233 | 10.7            | 43.2              | 1.300               | 0.200      | 0.300         | 1.300 | 0.065        | 0.100           | 3.00        | 1.300               | 0.124      | 0.117         | 1.300 | 0.022        | 0.035           | 0.38        |

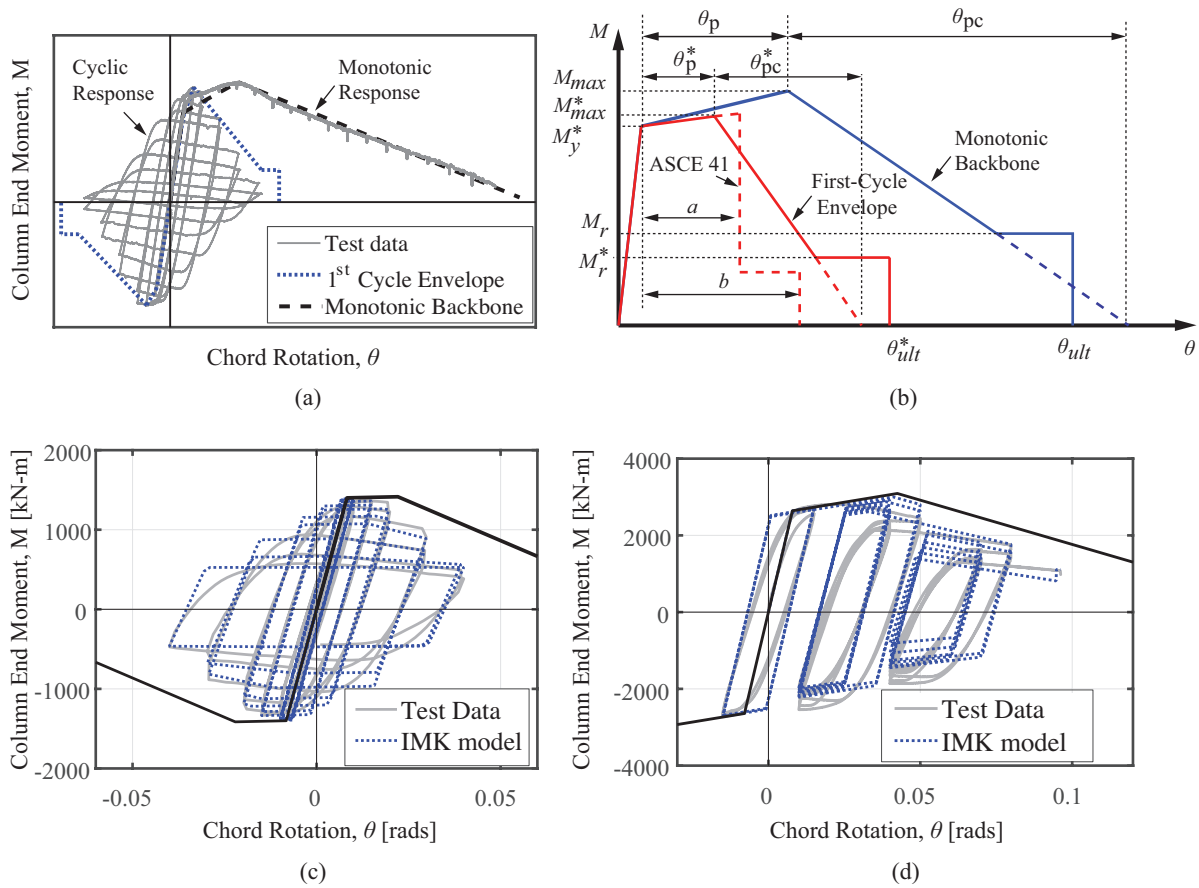


**Fig. 1.** Steel column component model definitions and illustrations of hysteretic deterioration model [Experimental data from Suzuki and Lignos (2015) and Elkady and Lignos (2018)a] (a) Monotonic and first-cycle envelope curves; (b) idealized monotonic backbone and first-cycle envelop curves; (c) Comparisons of measured and simulated column end moment versus chord rotation under symmetric loading history; (d) Comparisons of measured and simulated column end moment versus chord rotation under collapse-consistent loading history

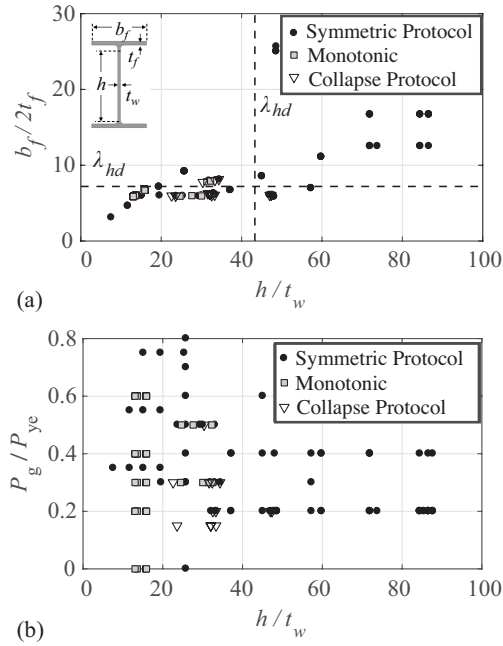


**Fig. 2.** Cross-section slenderness and axial load ratio ranges of the collected test data (compressive axial load ratio,  $P_g/P_{yc}$ , is indicated with a positive sign)

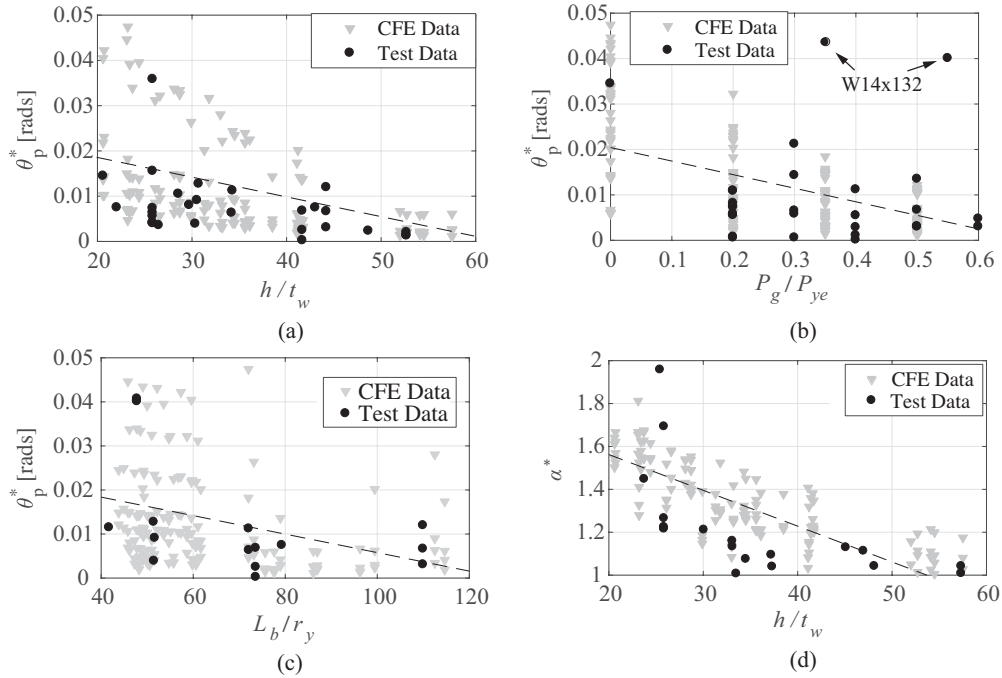
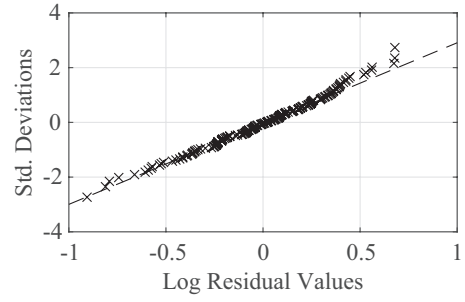
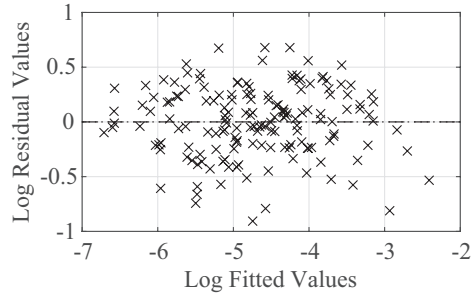


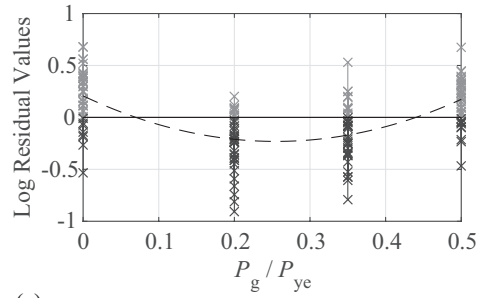
**Fig. 3.** Component model parameter trends based on symmetric cyclic loading histories



(a)



(b)



(c)

**Fig. 4.** Residual values from the regression analysis of pre-peak plastic rotation,  $\theta_p^*$

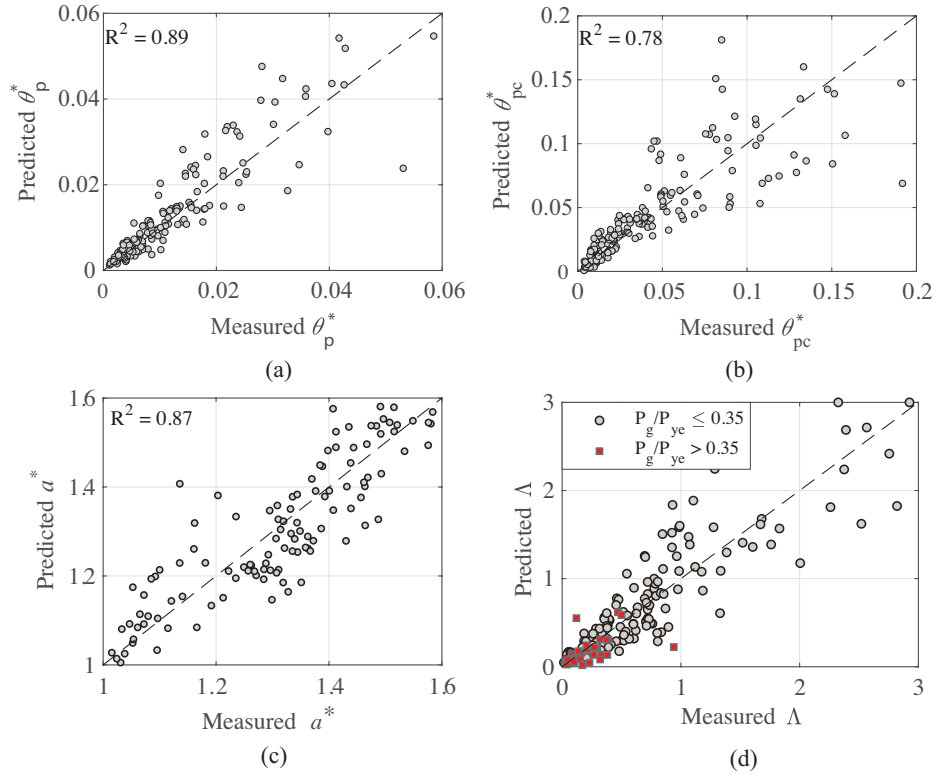


**Fig. 5.** Comparison of measured and predicted responses for selected component model parameters

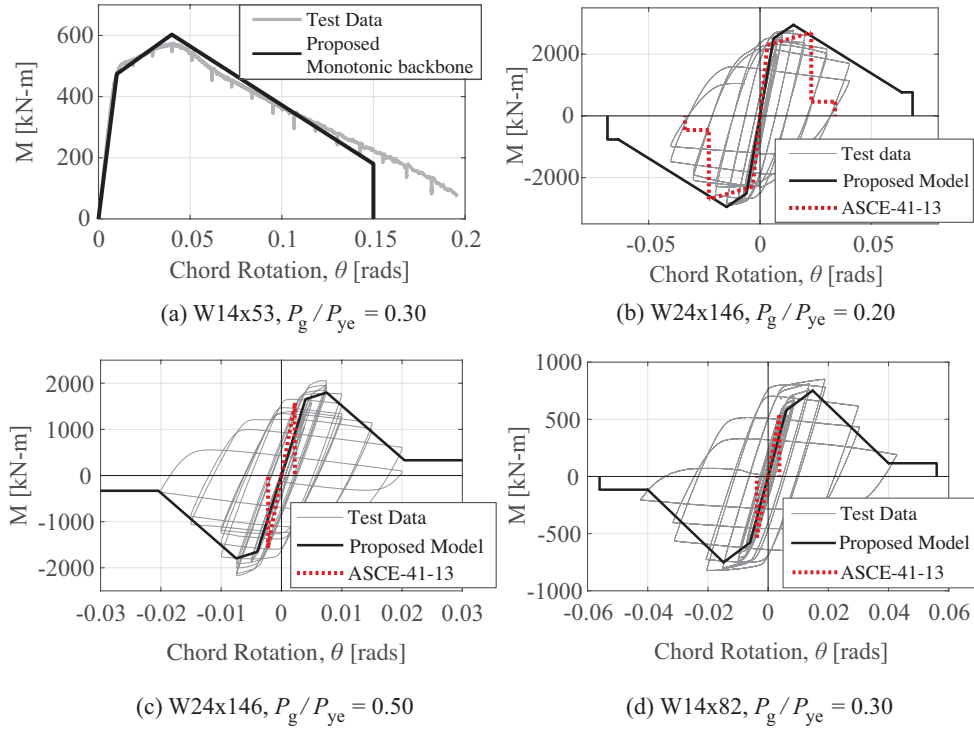


**Fig. 6.** Comparisons between test data, proposed component models, and ASCE 41-13 component modeling recommendations for steel wide flange columns [data from Suzuki and Lignos (2015) and Elkady and Lignos (2018)]

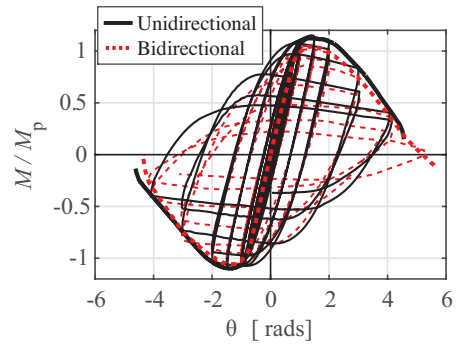
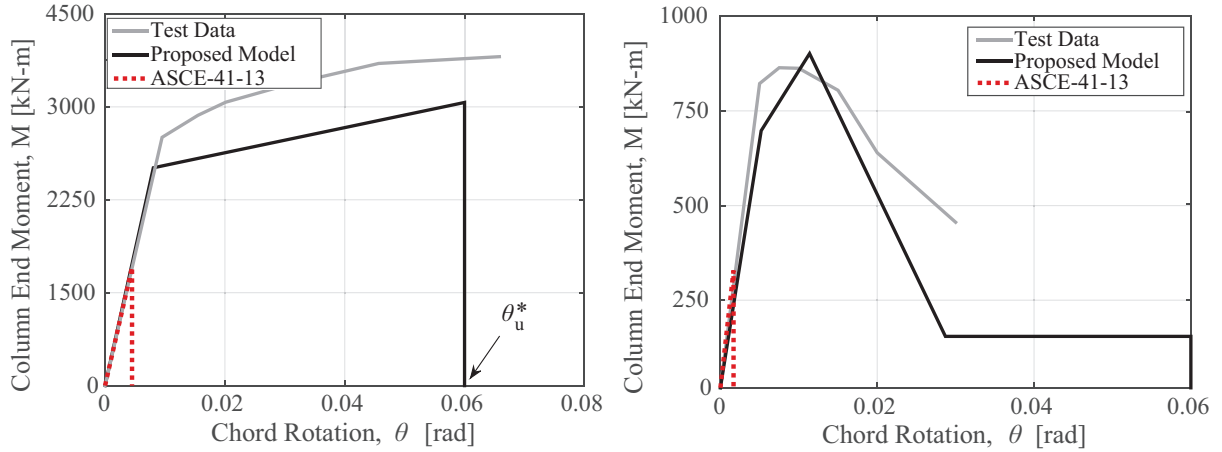
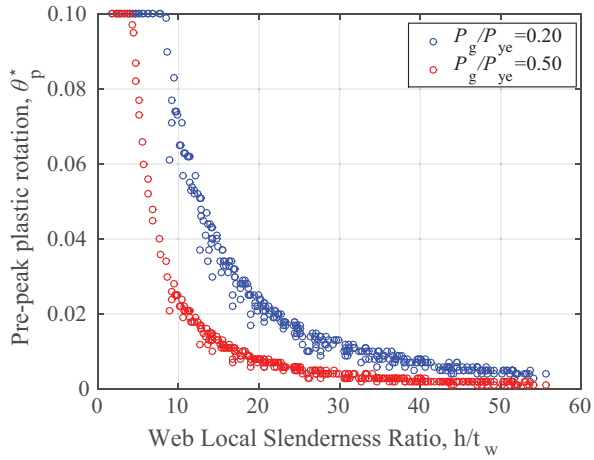


**Fig. 7.** Wide-flange steel columns (W24x84) subjected to unidirectional and bidirectional lateral loading [data from Elkady and Lignos (2018)]

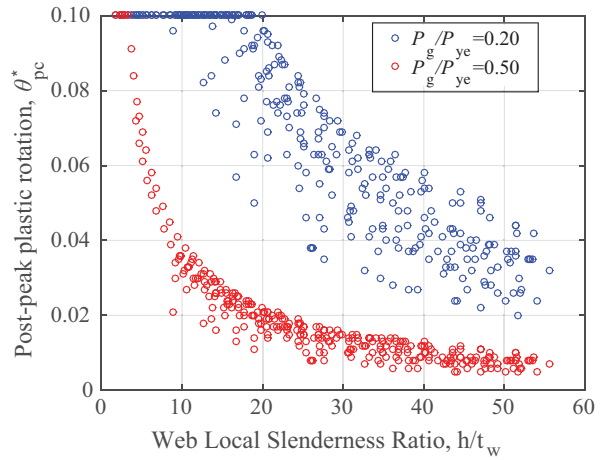


(a) W14x233-55,  $P_g/P_{ye} = 0.15$ ,  $P/P_{ye} \sim -0.15 - 0.75$  (b) W16x89,  $P_g/P_{ye} = 0.50$ ,  $P/P_{ye} \sim 0.25 - 0.75$

**Fig 8.** Comparisons of proposed modeling recommendations with ASCE 41-13 for end columns in steel MRF systems [data from Lignos et al. (2016); Newell and Uang (2008)].



(a)



(b)

**Fig. 9.** Trends of pre- and post-peak plastic rotations with respect to the cross-section web local slenderness ratio for modeling the first-cycle envelope curve of steel wide-flange columns